# Experiments with shell structure in metal clusters

S. Bjornholm, J. Borggreen, K. Hansen, T. Martin, T.D. Ramussen, J. Pedersen

# Experiments with Shell Structure in Metal Clusters

*S. Bjørnholm*[1], *J. Borggreen*[1], *K. Hansen*[1],
*T. Martin*[2], *H.D. Rasmussen*[1] *and J. Pedersen*[1],
The Niels Bohr Institute, Copenhagen[1],
Max-Planck-Institut für Festkörperforschung, Stuttgart[2]

**Résumé:** Les électrons de conduction à l'intérieur d'une gouttelette métallique forment un système quantique dont la structure est analogue à celle du noyau atomique. Les gouttelettes forment un système périodique entier des "noyaux-géants". Ceci s'explique à partir de la règle de quantisation de Bohr, appliqué aux électrons en mouvement classique à l'intérieur de la gouttelette en orbites triangulaires et carrés.

**Abstract:** The conduction electrons in small metal drops form ordered quantum states in analogy to the nucleons in the nucleus. The droplets form an entire periodic system of "giant nuclei" that can be understood by applying Bohr's quantization rule to electrons moving classically inside the droplets in triangular and square orbits.

## Introduction

Free and independent electrons bonded by the spherical surface of a small metallic drop will quantize into a total quantum state that exhibits shell structure[1-5]. There is here an analogy to the atomic electrons surrounding the nucleus and even more, an analogy to the ordering of protons and neutrons in the nucleus itself as described by the nuclear shell model[6]. The most significant difference is the absence of any spin-orbit splitting in the metal clusters. In the study of how metallic clusters grow, one therefore leans heavily on theories and experience from atomic and in particular from

nuclear physics [7,8]. In addition, since metal clusters readily exceed nuclei in the number of elementary constituents they contain, the metal clusters provide a basis for significant extensions of the quantum many body concepts developed to describe nuclear shell structure.

We shall here present measurements of the size distribution of sodium metal clusters, with up to 3000 atoms per cluster, obtained by expanding hot sodium vapour through a fine nozzle. Steps in the abundance distributions occur locally at sizes that differ in radius by 0.61 $r_{WS}$, where $r_{WS}$ is the Wigner-Seitz radius (i.e. radius of sphere representing the volume available to each atom or electron). For a cold electron gas the Pauli exclusion principle imposes a unique relation between $r_{WS}$ and the most energetic (Fermi) electron. The action of a classical electron moving with this energy will increase by one Planck unit $h$ for each increment in radius of the above magnitude, provided it moves inside the cluster surface in something intermediate between a closed triangular and a closed square orbit. Quantization of such classical closed orbits can therefore explain the observed periodicity. The experimental data further show clear evidence of a quantum beat mode, reflecting alternating constructive and destructive interference between quantized triangular and square orbits, respectively. The altogether 22 shell periods observed are divided into two groups separated by a minimum in the amplitude of the shell effect. In addition one sees a shift in phase in going from group one to group two, as expected for a beat mode.

## The experiment

Metal droplets are produced by expansion of metal vapour through a fine nozzle, the same way water droplets are formed by letting steam through a valve, Fig. 1.

The sodium vapour is generated in a stainless steel vessel held at 700-800 °C and the expansion is assisted by pressurizing the vessel with a large surplus of argon or xenon gas. The mixture is expanded into a three meter long, differentially pumped flight tube, resulting in a narrow beam of free-flying metal clusters with velocities close to the initial thermal speed of the

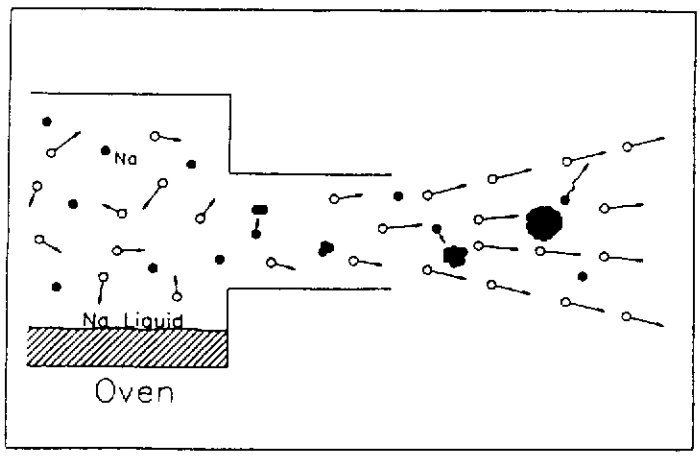


*Fig. 1* - **Production of sodium clusters, i.e. giant atoms.** *In the expansion of an inert gas through a 0.1 -0.2 mm diameter nozzle, random thermal motion is converted to uniform translational motion, resulting in strong cooling of the inert gas. Introducing atomic sodium vapor into this medium, the sodium atoms aggregate into clusters with a broad, uniform size distribution.*

argon or xenon atoms. In the expansion and clustering process, lasting about 100 nanoseconds, the noble gas medium cools to a few tens of Kelvin. In the sodium clusters, on the other hand, there will be a competition between heating, due to condensation, and cooling, due to collisions. We believe that the resulting internal temperature in the freshly formed clusters is just some 100-200 °C below the oven temperature. In the ensuing free flight for about one millisecond the droplets will therefore loose sodium atoms by stepwise evaporation, cooling to about 100-200 °C. This evaporation process is sensitive to shell-like variations in the atomic separation (free) energies; and these variations are thought to be responsible for the step-like modifications of the experimentally observed size distributions, while presumably the pre-evaporation size distributions are completely uniform.

One meter downstream the size distribution is sampled by time-of-flight mass spectrometry. Ultraviolet photons with energies just about the ionization threshold and an energy spread of 1 eV (compared to a total Fermi energy

in sodium of 3.24 eV), are used to produce a representative sample, in the form of ions, from the otherwise neutral size distribution. Figure 2, upper part, shows an example of an abundance distribution $I_N$ vs. $N$ obtained in this way. The quantity $N$ is the number of atoms or conduction electrons in the cluster.

## Magic numbers

One sees clearly in Fig. 2 how the global bell-shaped distribution is scarred with saw-tooth or $s$-shaped irregularities at certain "magic" sizes.

Since the interest focusses on these, it is convenient to display the experimental result in terms of relative intensity changes, i.e.:

$$\Delta_1 \ln I_N = \ln(I_{N+1}/I_N) \approx 2\,\frac{(I_{N+1} - I_N)}{(I_{N+1} + I_N)}\,. \qquad (1)$$

As one sees from Fig. 2, lower part, this makes the magic numbers stand out very clearly as dips in the curve. At the same time, one sees how the dips become smaller and broader with increasing magic number, $N_\circ$. For higher $N_\circ$-values the dips signalling shell closures will drown in noise due to finite counting statistics. In this situation we have found it useful to make a compromise between "band pass" in terms of the size interval sampled and statistical noise, by computing a properly weighted logarithmic derivative for properly spaced mass points $N$,

$$\langle \Delta_1 \ln I_N \rangle_{K_\circ} = \frac{\sum_{K=2K_\circ/3}^{K_\circ} 2\,\dfrac{(I_{N+1+K} - I_{N-K})(2K+1)}{I_{N+1+K} + I_{N-K}}}{\sum_{K=2K_\circ/3}^{K_\circ} (2K+1)^2}\,, \qquad (2)$$

choosing values of $K_\circ = 0.03\,N$. The derivative is thus sampled over intervals of $2K_\circ + 1$, i.e. $\pm 3$ % of the actual size. In this way it becomes realistic to scale up the measured derivatives in order to display very small irregularities

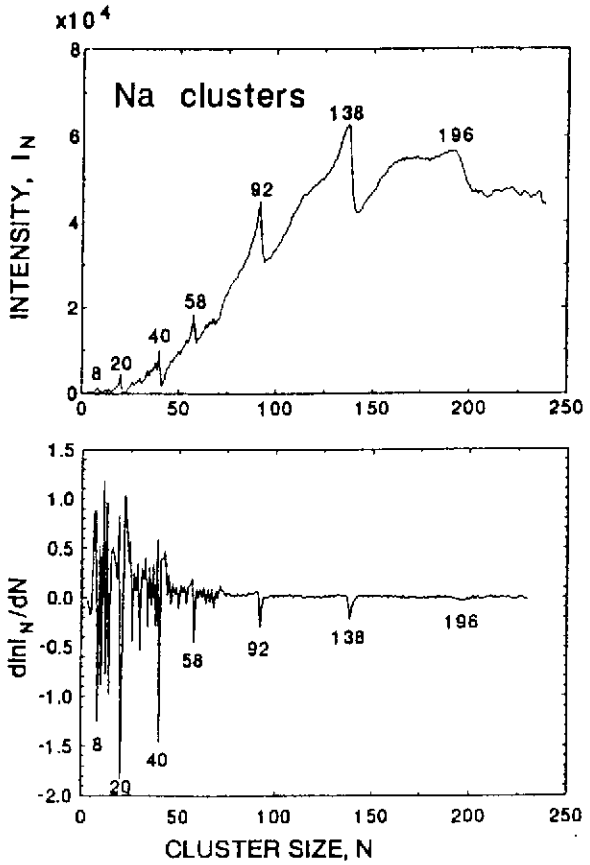


*Fig. 2* - **Mass spectra.** *Top panel: Abundance distribution for sodium clusters produced by adiabatic expansion and measured after a one meter free flight by time-of-flight mass spectrometry. In this measurement the individual mass peaks are fully resolved. Each point represents the integrated mass peak, corrected for background. Bottom panel: Logarithmic derivative* $\Delta_1 \ln I_N$ *of the results in top panel according to eq. (1).*

in the intensity pattern. Figure 3 shows the results, plotted as a function of the linear dimensions of the clusters, $\sim N^{1/3}$. At each dip the magic number $N_o$ is indicated. The dips are very nearly equidistantly spaced in the plot (Fig. 3), indicating that each new period require the same increment in drop radius $\Delta R = r_{ws}\, \Delta N_o{}^{1/3}$ to be completed.

A closer test of the linearity is made in Fig. 4, where $N_o{}^{1/3}$ is plotted

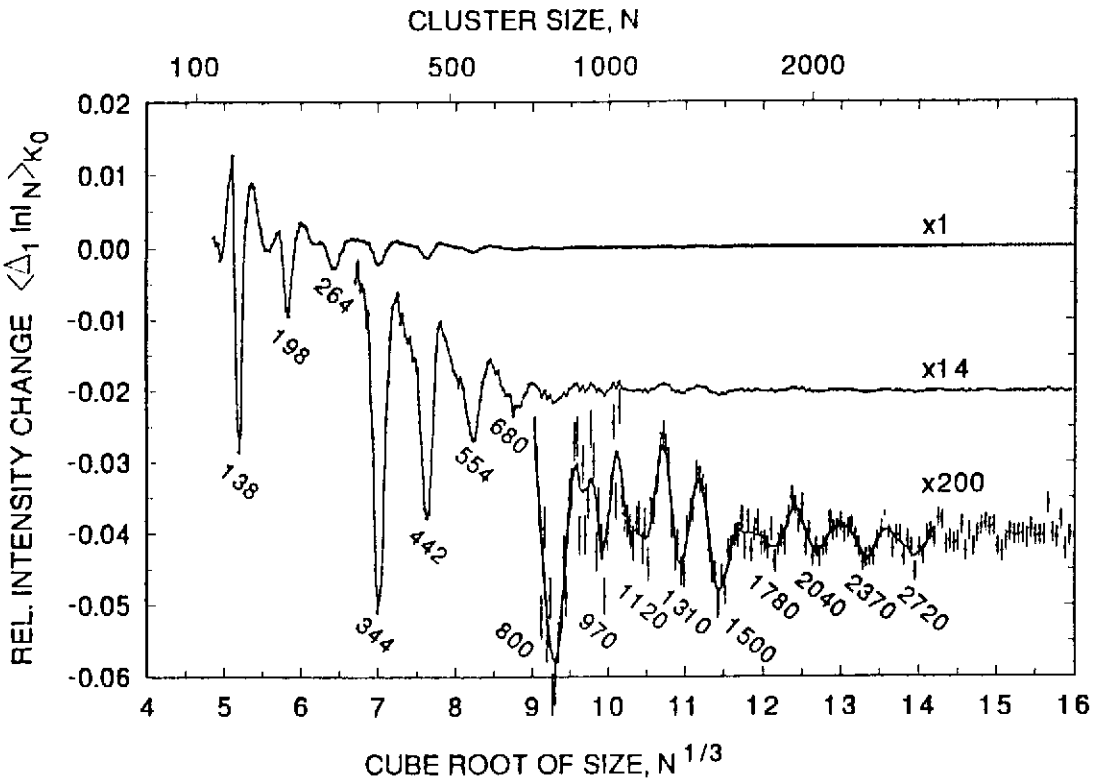


*Fig. 3* - **Magic numbers.** *Relative changes in the cluster abundance distributions, $\langle\Delta_1 \ln I_N\rangle_{K_0}$, calculated from the measured mass abundance spectra $I_N$ according to eq. (2) and plotted as a function of $N^{1/3}$. In these measurements the individual masses are not resolved in the time-of-flight spectra. Time-of-flight is converted to mass by extrapolation from the low-mass region, where peaks are resolved, and the intensity per mass $I_N$ calculated without background correction. (Some background originates from doubly ionized clusters. This has been kept at a minimum by adjustment of the ionizing light intensity to a relatively low level).*

against a running index $n$, accounting for the period (or shell) number.

From the slope of the straight lines in Fig. 4 one finds that the increment in radius per period is $\Delta R = (0.61 \pm 0.01)\ r_{ws}$. The increment $\Delta L$ in circumference $2\pi\Delta R$ is then $(3.83 \pm 0.06)\ r_{ws}$. The de Broglie wavelength of an electron with the Fermi energy[9] is $\lambda_F = (32\pi^2/9)^{1/3}\, r_{ws} = 3.28\, r_{ws}$, which is not so far from the increment in the circumference or, equivalently,

in the length of a full circular orbit. However, triangular and square orbits are in much closer agreement with the de Broglie quantization rule $\Delta L = \lambda_F$, having length increments of $3\sqrt{3}\Delta R = (3.17 \pm 0.06) r_{ws}$ and $4\sqrt{2}\Delta R = (3.45 \pm 0.06) r_{ws}$, respectively. This is the first very significant observation resulting from simply measuring the positions $N_o$ of the dips in Fig. 3.

The second result is the observation, Fig. 4, that the magic numbers, or rather the $N_o{}^{1/3}$-values, fall on two straight lines displaced by one-half unit of $n$, the shell index. The sum of two cosine functions of $n$ with some 7-10 % difference in wave numbers $k_\triangle$ and $k_\square$, respectively would show such a phase shift:

$$\cos(k_\triangle n) + \cos(k_\square n) = 2\cos\left(\frac{k_\triangle + k_\square}{2} n\right) \cos\left(\frac{k_\triangle - k_\square}{2} n\right) . \quad (3)$$

Combined with the first result, this strongly suggests that quantized triangular and square orbits together are responsible for the observed periodicities in the abundance distributions.

## Intensities

An interference pattern of the type eq. (3) should show up as a long wavelength modulation of the short wavelength periodicities visible in Figs. 2 and 3. Instead, one sees there a seemingly monotonous decrease in the amplitudes of the shell dips. There are two reasons for this decrease.

Shell structure is due to periodic variations in an otherwise uniform single particle electron level density. In a constant density medium with constant Fermi energy, or, equivalently, constant width of the conduction band, the spacing $\hbar\omega_{shell}$ between consecutive modulations must decrease as $1/n$. This will cause an $N_o{}^{-1/3}$ decrease in the expected dips. If furthermore the amplitudes of the shell modulations decrease as $N_o^{-1/6}$, one arrives[8] at a decrease varying as $N_o^{-1/2}$ – even at zero absolute temperature.

The other, more important, reason for the strongly decreasing dip amplitudes

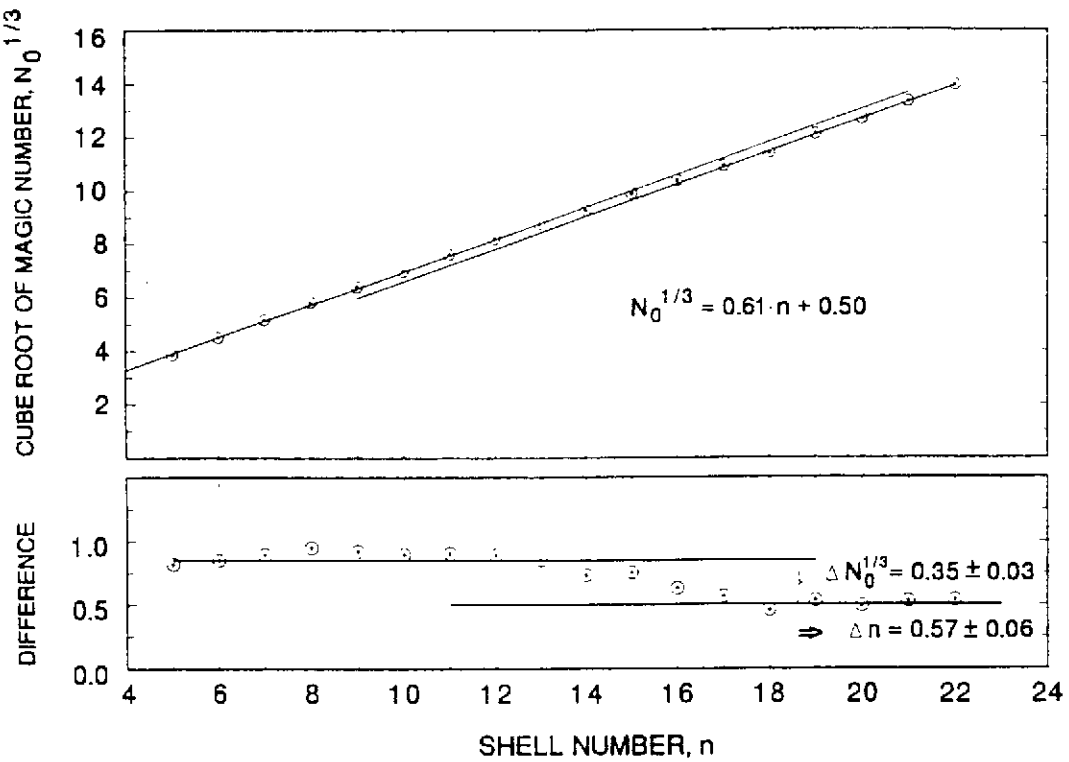


*Fig. 4* - **The phase shift**. *Cube root of the magic numbers from Fig. 3, signifying shell closures, plotted against shell number n. (Top panel). For higher shell numbers the points fall on two straight lines, phase-shifted by one half shell number. This is shown more clearly in the panel below where the points result from subtraction of a straight line from the data above.*

is temperature[10-12], which tends to wash out the observable shell structure – exponentially[8] in the effective temperature parameter $\tau$,

$$\tau = k_B T \frac{2\pi^2}{\hbar\omega_{shell}} , \tag{4}$$

with

$$\hbar\omega_{shell} \approx 2\varepsilon_F/n \propto N^{-1/3} . \tag{5}$$

Here $k_B$ is Boltzmann's constant, $T$ is the real temperature at the time of

sampling the abundance distributions, estimated[13] to be 400-500 K, while $\varepsilon_F = 3.24$ eV is the Fermi energy.

In order to compensate for these effects we have scaled the experimental logarithmic derivatives, $\langle \Delta_1 \ln I_N \rangle_{K_0}$ cf. Fig. 3, with the factor $N^{1/2} \exp(cN^{1/3})$, setting $c = 0.65$. The result is presented in Fig. 5.

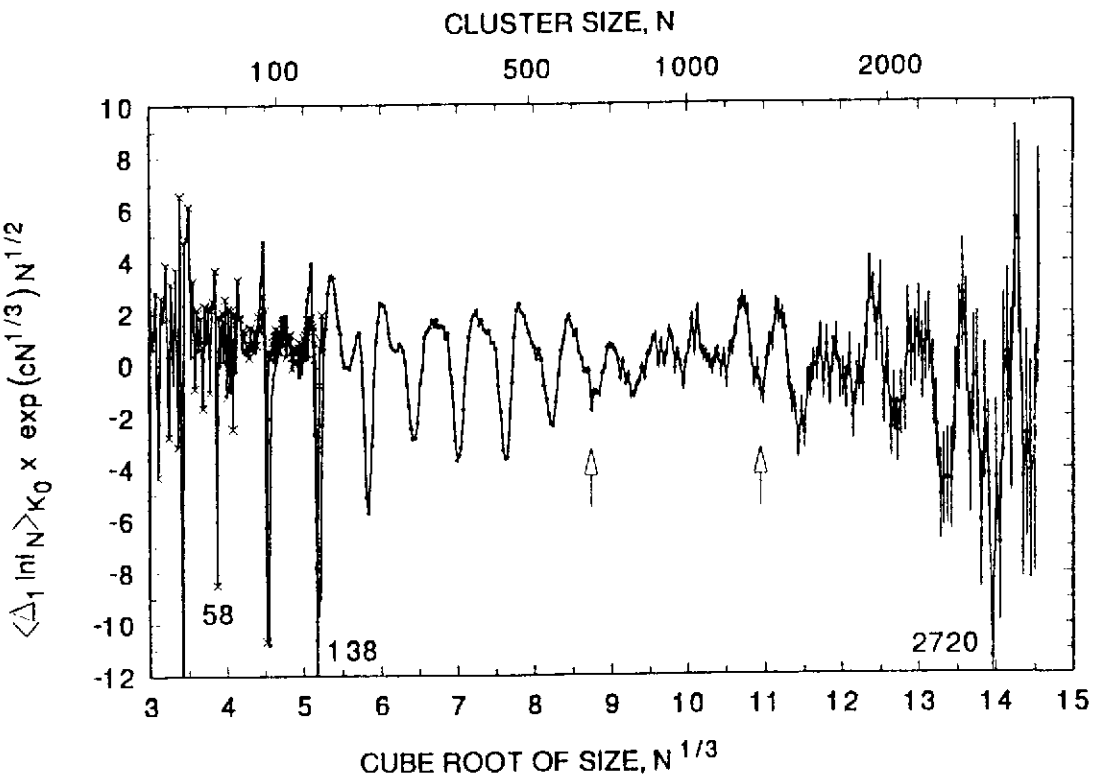


*Fig. 5* - **The quantum beat.** *Relative changes* $\langle \Delta_1 \ln I_N \rangle_{K_0}$ *in experimental cluster abundance* $I_N$*, corrected for the effect of temperature and shell compression, as a function of linear cluster dimensions* $N^{1/3}$*. The model considerations behind these corrections are described in refs.*[8,10–12]*. The highest shell in the first group (supershell) according to the phase shift plot, Fig. 4, and the first shell in the second group are indicated by arrows. The measurements from Fig. 2, lower part, are also shown (crosses). The logarithmic amplitudes* $\Delta_1 \ln I_N$ *are here summarily scaled by an extra factor of 0.2 to account for the superior mass resolution and the use of eq. (1) instead of eq. (2) for these data.*

Since the scaling function is monotonously increasing, it cannot by itself

introduce the large scale modulations seen in the plot. They indeed have the character of a beat mode as expected from eq.(3) and from the results of the previous section.

Correcting the experimental abundance modulations for the influence of finite temperature and for the compression of the shells with increasing size thus corroborates the previous results, obtained solely by examining the sequence of magic numbers.

## The quantum beat

From this analysis one obtains an understanding of the periodic abundance variations with cluster size as the result of quantization of triangular and square electron orbits inside the sodium droplets, in the spirit of Bohr[14] and de Broglie[15]. The presence of two orbits, and hence two slightly differing periods, results in a beat pattern superposed on the "fundamental", primary shell periodicity. The beat mode has a minimum around shell no. 16, where there are about 1100 conduction electrons in the cluster. An illustration of how the combination of "preferred" cluster radii for electrons orbiting with equal energy in triangular and square orbits, respectively, can lead to an interference pattern[16] is given in Fig. 6.

## Modern theories

The attempt to discuss the experiment in the simplest possible terms is deliberate. It does not imply that modern quantum theories have overlooked the effects shown or are inadequate for their description. Indeed, we were inspired by several newer theories of shell structure in nuclear systems, in particular refs.[8,17], in first mounting the experiment. Also, the prior theoretical treatment of size and temperature effects[8], have guided the analysis of the admittedly very weak abundance modulations. Some theoretical developments[10,11,18] have occurred in parallel with the experimental campaign, helping to sharpen and focus the effort.

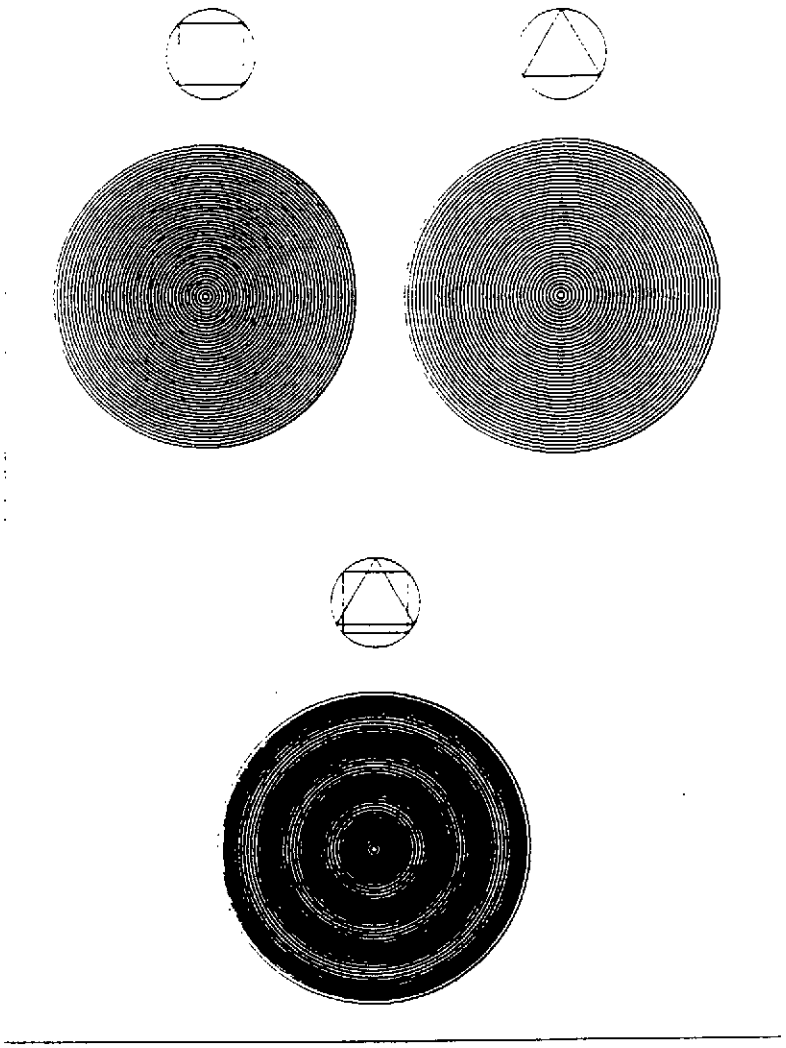

*Fig. 6* - **Correspondence principle.** *For a particle with Fermi-energy, triangular orbits will have integer action values for a set of discrete drop radii (top right). Analogously, square orbits require another set of discrete radii in order for the action to be an integer multiple of h (top left). The drop sizes that meet both requirements exhibit a beat pattern (bottom center).*

The modern theories[18] are particularly helpful in answering why just two orbits, triangles and squares, suffice to understand the experiment, and why pentagons, hexagons, etc., etc. can be neglected. In a more complete theory, all closed orbits indeed contribute to the final spectrum of discrete quantal energy eigenstates. But the experiment averages over this forest of discrete

states, being only sensitive to the gross features in the level density, and these features are found to be dominated by contributions from the two shortest closed orbits (with non-zero angular momentum).

## Particles and waves

Periodicities due to quantum shell structure have been identified in a large number of experiments[1,2,19,20], the most recent one[21] extending to cluster sizes almost as large as the ones described here. Of special interest is ref.[19]. Working with cold sodium clusters at about 100 $K$, the authors find quantum shell periodicities for clusters with 1400 atoms or less, while periodicities in the size interval from $N = 1400$ all the way up to $N = 20000$ give evidence of geometrical packing of sodium ions into icosahedral quasicrystals. This last aspect has no analogue in nuclear systems and is an example of the coexistence in one experiment of wave-order and particle-order, respectively. Combined with the present, high-temperature experiment it also illustrates how the periodicities that one encounters in connection with the growth of clusters towards macroscopic dimensions can depend rather strongly on temperature, reflecting basically the difference between soft (perhaps liquid) and solid end products.

The authors wish to thank O. Echt, W.D. Knight and B.R. Mottelson for most valuable advice and encouragement.

## References

1. W.D.Knight, K. Clemenger, W.A. de Heer, W.A. Saunders, M.Y. Chou, and M.L. Co: :n, *Phys. Rev. Lett.* **52**, 2141 (1984), and W.A. de Heer, W.D. Knight, M.Y. Chou, and M.L. Cohen, *Solid State Physics* **40**, 93 (1987)
2. I. Katakuse, T. Ichihara, Y. Fujita, T. Matsuo, T. Sakurai, and H. Matsuda, *Int. J. Mass Spectrom. Ion Proc.* **67**, 229 (1985)
3. W. Ekardt, *Phys. Rev.* **B29**, 1558 (1984)
4. O.E. Beck, *Solid State Commun.* **49**, 381 (1984)
5. M.Y. Chou, and M.L. Cohen, *Phys. Lett.* **A133**, 420 (1986)

6. M.G. Mayer, and J.H.D. Jensen, *Elementary Theory of Nuclear Shell Structure*, 1 (Wiley, New York, 1955)
7. A. Bohr, and B.R. Mottelson, *Nuclear Structure*, Vol. **I**, 2 (Benjamin, New York, 1969).
8. A. Bohr, and B.R Mottelson, *Nuclear Structure*, Vol. **II**, 2 (Benjamin, London, 1975)
9. N.W. Ashcroft, and N.D. Mermin, *Solid State Physics*, 1 (Saunders College, Philadelphia, 1976).
10. M. Brack, O. Genzken, and K. Hansen, *Z. Phys.*, to appear (1991)
11. M. Brack, O. Genzken, and K. Hansen, *Z. Phys.*, to appear (1991)
12. S. Bjørnholm, J. Borggreen, O. Echt, K. Hansen, J. Pedersen, and H.D. Rasmussen, *Z. Phys.* to appear (1991)
13. C. Brechignac, Ph. Cahuzac, J. Leygnier, and J. Weiner, *J. Chem. Phys.* **90**, 1492 (1989)
14. N. Bohr, *Phil. Mag.* 26, 1 (1913)
15. L. de Broglie, *C.R. Acad.Sci.Paris*, **179**, 39 and 676 (1924)
16. S. Bjørnholm, in *Clusters of Atoms and Molecules* (ed. Haberland, H.) Ch. 2.4, pp.24 (Springer, Berlin, to appear 1991)
17. R. Balian, and C. Bloch, *Ann. Phys.* **69**, 76 (1972)
18. H. Nishioka, K. Hansen, and B.R. Mottelson, *Phys. Rev.* **B42**, 4377 (1990)
19. T.P. Martin, T. Bergmann, H. Göhlich, and T. Lange, *Chem. Phys. Lett.* **172**, 209 (1990)
20. S. Bjørnholm, J. Borggreen, O. Echt, K. Hansen, J. Pedersen, and H.R. Rasmussen, *Phys. Rev. Lett.* 65, 1627 (1990)
21. T.P. Martin, S. Bjørnholm, J. Borggren, C. Bréchignac, P. Cahuzac, K. Hansen, and J. Pedersen, *Chem.Phys.Lett.* submitted (1991)

texsb220391a